JOURNAL OF MATERIALS SCIENCE 26 (1991) 6729–6735

Characterization and thermal behaviour of praseodymium tartrate crystals grown by the silica gel technique

V. MANSOTRA, K. K. RAINA, P. N. KOTRU*, M. L. KOUL‡
Department of Physics and Chemistry‡, University of Jammu, Jammu–180 001, India

Results of EDAX, XRD, IR, TG, DSC and SEM carried out on crystalline materials obtained by diffusion of praseodymium ions through silica gel impregnated with tartaric acid are reported. The crystallized material assumed spherulitic morphology which was established to be $Pr_2(C_4H_4O_6)_3 5H_2O$. EDAX confirmed the presence of praseodymium. X-ray diffraction data giving 2θ, intensity and *d*-values is also reported for the first time. Infrared spectrum in the range of 500–4000 cm^{-1} and the description of peaks recorded for the material are given. Results of thermal analysis (TG and DSC) indicated that the material is thermally unstable; the decomposition only occurs at 40–560 °C, after which it reduces to Pr_2O_3. SEM results suggest spherulitic growth arising from diverging crystal fibres which originate from multiple nuclei dispersed within a centrally-located spherical region.

1. Introduction

There is considerable interest in the physical properties, especially optical and magnetic, of materials involving rare-earth ions. Many materials containing the rare-earths have been grown as single crystals by the flux method and are suitable for investigations of magnetic, optical and mechanical properties [1–10]. McCauley and Gerhardt [11] reported the growth of neodymium carbonate from silica gel. Kotru *et al* [12–21] have reported extensive investigations on the growth and characterization of rare-earth tartrates (R = La, Gd, Dy and Di)§ grown in silica gels.

In this paper we report the results obtained on characterization of praseodymium tartrate by X-ray diffraction, infrared spectroscopy, qualitative elemental analysis using EDAX, scanning electron microscopy and thermoanalytical techniques, such as thermogravimetry (TG) and differential scanning calorimetry (DSC).

1.1. Crystal growth

The crystals of praseodymium tartrate were grown by allowing praseodymium ions to diffuse through silica gel impregnated with tartaric acid. Crystallization leads mostly to spherulitic morphology of praseodymium tartrate pentahydrate. The details of growth are reported elsewhere [22].

2. Results and discussion

2.1. EDAX results

Identification of the rare-earth constituents of the material was carried out by qualitative elemental analysis using EDAX. Fig. 1 shows an EDAX curve of praseodymium tartrate. The peaks attributed to the presence of praseodymium at different energies are depicted. The Au peak is due to gold plating of the sample.

2.2. X-ray diffraction

Fig. 2 shows the X-ray diffractogram of praseodymium tartrate crystals and the computed XRD data is given in Table I. The characteristic X-ray data on this material is reported for the first time. To the best of the authors' knowledge, there is no X-ray diffraction data on these crystals available in the literature [23].

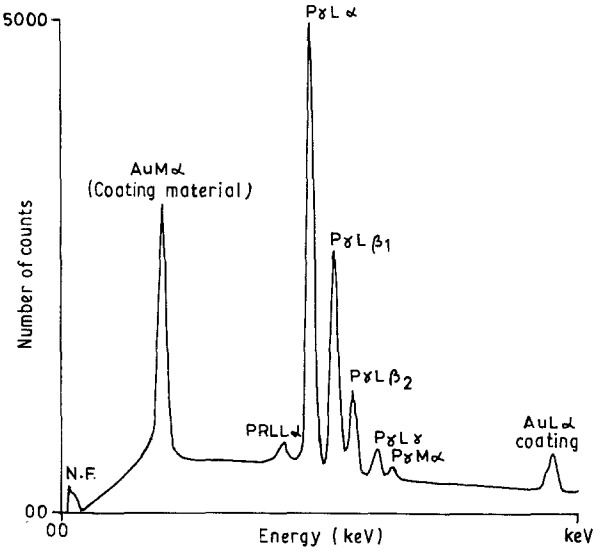

Figure 1 EDAX curve of praseodymium tartrate showing the presence of Pr.

*To whom all correspondence should be addressed.
§Di (Didymium) is a mixture of rare-earths (La, Nd, Pr and Sm)

0022–2461/91 $03.00 + .12

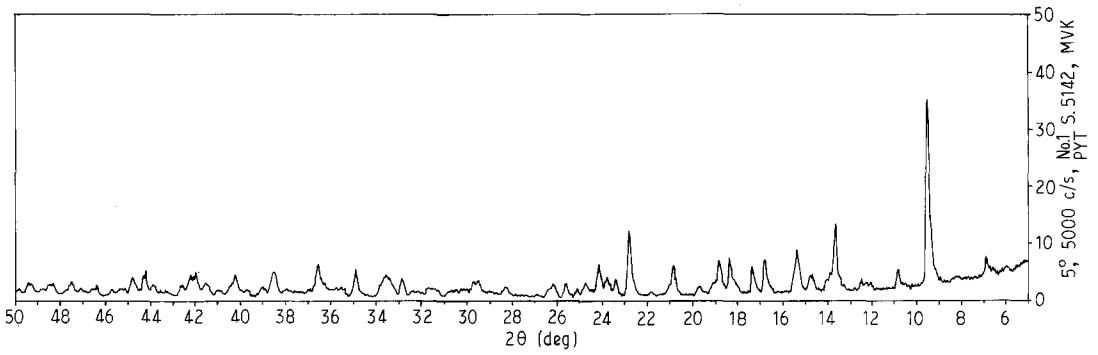

Figure 2 X-ray diffractogram of $Pr_2(C_4H_4O_6)_3 \cdot 5H_2O$.

TABLE I X-ray powder data of $Pr_2(C_4H_4O_6)_3 \cdot 5H_2O$

Intensity values	2θ	*d* values (nm)
7.5	6.9	1.279963878
35.0	9.5	0.9301614214
5.0	10.8	0.8184717937
13.0	13.6	0.6505271833
4.5	14.7	0.6020863668
9.0	15.4	0.5748726987
7.0	16.8	0.5272686414
6.0	17.4	0.509197694
7.5	18.4	0.4817639989
7.0	18.8	0.4716029157
6.0	20.8	0.4266860443
12.5	22.8	0.3896895499
6.5	24.2	0.3674531441
4.5	33.5	0.2672657786
5.5	34.9	0.2568583856
6.0	36.5	0.2459575417
5.0	38.5	0.231896467
4.5	40.5	0.2241316082

2.3. Infrared spectroscopy

Fig. 3 is the characteristic infrared spectrum of $Pr_2(C_4H_4O_6)_3 \cdot 5H_2O$ in the range of 500–4000 cm^{-1}. There is a very strong peak at 3400 cm^{-1} due to water and the OH stretching mode. A band at approximately 1560 cm^{-1} is attributed to the C=O stretch of the carbonyl group. A strong peak at 1380 cm^{-1} is due to C=O symmetric + δ(O–C=O) modes. The weak and shoulder peaks at 1230 cm^{-1}, 1280 cm^{-1} and 1310 cm^{-1} are due to OH in the plane bending mode. The peaks of varying intensities at 1140 cm^{-1}, 1110 cm^{-1}, 1075 cm^{-1}, 1060 cm^{-1}, 990 cm^{-1}, 940 cm^{-1}, 880 cm^{-1} and 840 cm^{-1} are due to various types of C–H vibrating modes. The band near 700 cm^{-1} is due to crystal water as reported already in some other rare-earth tartrates [20]. The band assignment in the infrared spectrum was done by analogy with the infrared spectra of other rare-earth tartrates already published [17, 18, 20, 21]. The bands below

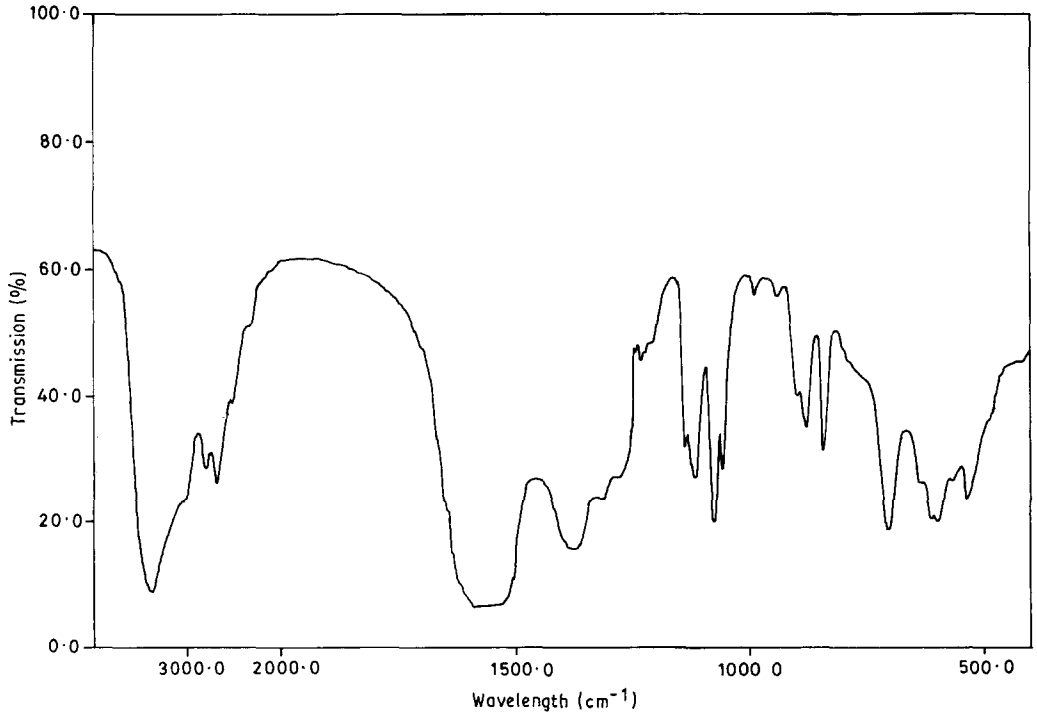

Figure 3 Characteristic infrared spectrum of $Pr_2(C_4H_4O_6)_3 \cdot 5H_2O$.

TABLE II Infrared band assignment for $Pr_2(C_4H_4O_6)_3 \cdot 5H_2O$

Band	Assignment
1. 3400 cm^{-1} (bs)	ν(OH) Water
2. 1560 cm^{-1} (bs)	ν(C=O)
3. 1380 cm^{-1} (bs)	ν(C=O) + δ(O–C=O)
4. 1310 cm^{-1} (w)	
5. 1280 cm^{-1} (w)	δ(OH)
6. 1230 cm^{-1} (w)	
7. 1140 cm^{-1} (s)	
8. 1110 cm^{-1} (s)	δ(C–H) + π(C–H)
9. 1075 cm^{-1} (s)	δ(C–H), π(C–H) and ν(C=O)
10. 1060 cm^{-1} (s)	coordinated C–OH group

600 cm^{-1} are due to metal oxygen bonds. Table II gives the details of the band assignments.

2.4. Thermal behaviour

The thermogram showing TG of praseodymium tartrate crystals is shown in Fig. 4. As indicated, the material starts decomposing at about 40 °C and the process continues up to 560 °C, after which it is reduced to its oxide. The first stage of decomposition (40–125 °C) results in the elimination of four water molecules. The calculated and actual weight losses corresponding to this are 8.83% and 10% of the total weight taken, respectively. The second stage between 145 to 185 °C corresponds to the loss of one water molecule and results in the formation of anhydrous praseodymium tartrate. The measured and theoretical values of weight losses in the process being 11.03% and 12% of the total weight taken, respectively. In the third stage between 204 and 310 °C, the anhydrous praseodymium tartrate is reduced to praseodymium oxalate. The measured and theoretical values of weight losses at this stage are 33.09% and 32% of the total weight taken, respectively. The fourth stage of decomposition (between 320–385 °C) results in the reduction of praseodymium carbonate; the measured and theoretical values of weight losses are 43.39% and 44%, respectively. In the fifth and final stage (between 412–560 °C) the praseodymium carbonate is reduced to an oxide; the measured and theoretical values of weight losses are 59.57% and 57%, respectively. Table III summarises the analysis of the decomposition steps in the TG, the corresponding weight losses

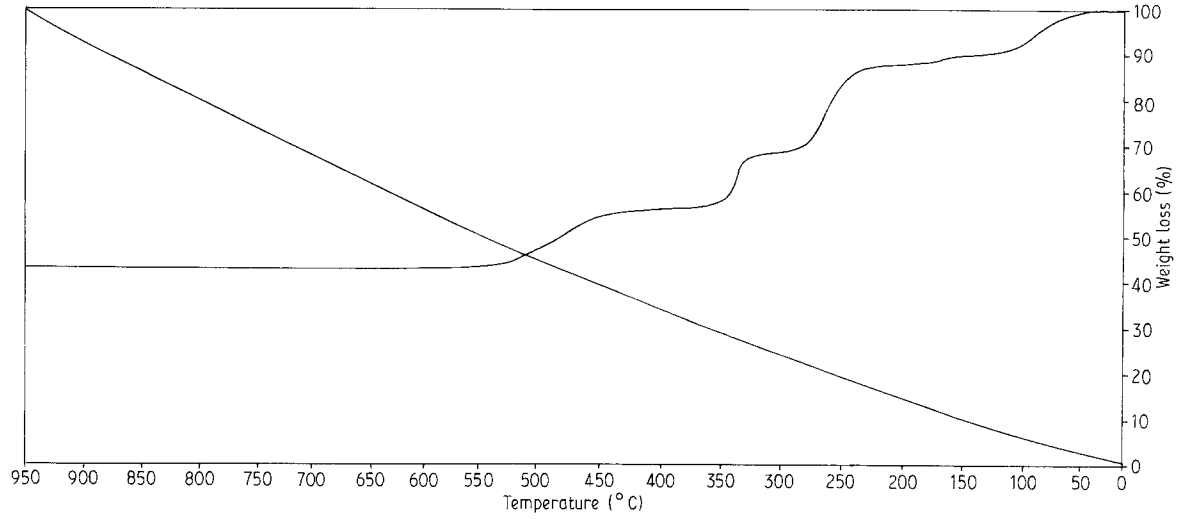

Figure 4 Recording of TG curve of $Pr_2(C_4H_4O_6)_3 \cdot 5H_2O$.

TABLE III Results of decomposition process of $Pr_2(C_4H_4O_6)_3 \cdot 5H_2O$

Stage	Decomposition temperature (°C)	Decomposition step	Calculated mass loss (%)	Actual mass loss (%)
1st	40–125	$Pr_2(C_4H_4O_6)_3 \cdot 5H_2O$ ↓ $Pr_2(C_4H_4O_6)_3H_2O$	8.83	10
2nd	145–185	$Pr_2(C_4H_4O_6)_3H_2O$ ↓ $Pr_2(C_4H_4O_6)_3$	11.03	12.0
3rd	204–310	$Pr_2(C_4H_4O_6)_3$ ↓ $Pr_2(C_2O_4)_3$	33.09	32.0
4th	320–385	$Pr_2(C_2O_4)_3$ ↓ $Pr_2(CO_3)_3$	43.39	44
5th	412–560	$Pr_2(CO_3)$ ↓ Pr_2O_3	59.57	57

and the temperature ranges. The thermal behaviour reported here is very similar to other rare-earth tartrates (R = La, Gd, Dy and Di) [16–18, 20, 21]. The total number of water molecules present in the composition was also independently established in the following manner.

The compound was heated in a tared crucible in an oven to 800 °C and kept at that temperature for an hour. The difference between the initial and final weights gave the weight loss due to loss of water and decomposition of the anhydrous compound to the final product Pr_2O_3. The weight of the end product thus formed corresonds very well to the stoichiometry of the compound *viz.* $Pr_2(C_4H_4O_6)_3 \cdot 5H_2O$.

Fig. 5 shows the DSC curve recorded for praseodymium tartrate. Critical examination of the TG and DSC curves indicate that the transformations are associated with mass changes and there is no physical (crystallographic) transformation independent of mass change or decomposition of the material.

2.5. Scanning electron microscopy

The spherulitic morphology observed for praseodymium tartrate crystals can be categorised under two headings: (1) Normal-type (NT) spherulites and (2) spiky-type (ST) spherulites. In order to reveal the finer details of the morphology of these crystals, they were studied under scanning electron microscope. Fig. 6(a) and (b) are the scanning electron micrographs of a ST-spherulite at different magnifications. From Fig. 6(a) it appears as if the crystal fibres are diverging radially from the centre of the spherulite. However, a look at the higher magnification (Fig. 6(b)) reveals that the fibres diverge radially from the centre but not from a single nucleus. The central region of the spherulite is

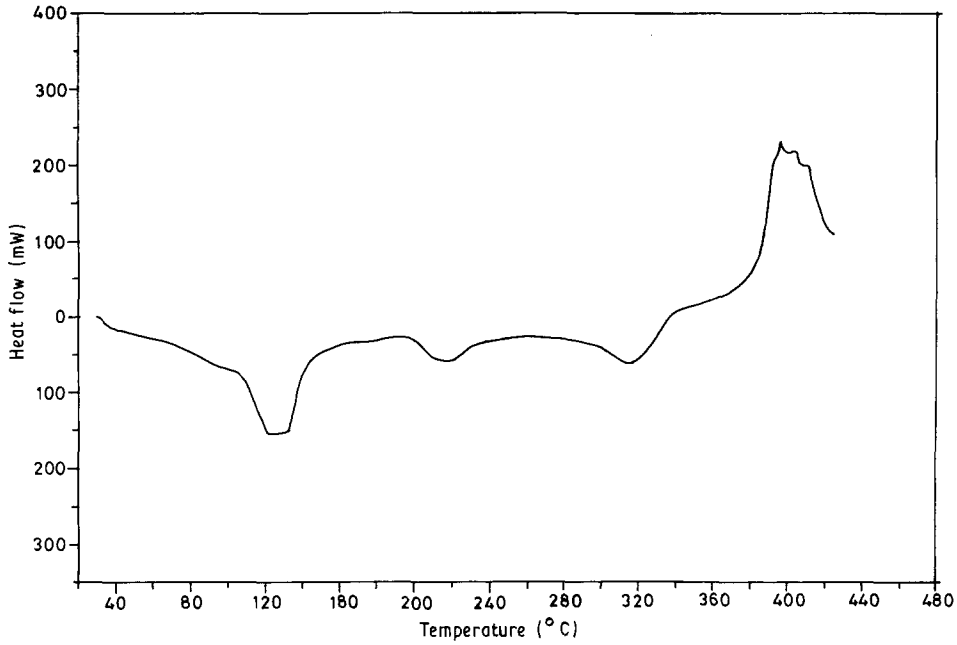

Figure 5 Recording of DSC curve of $Pr_2(C_4H_4O_6)_3 5H_2O$.

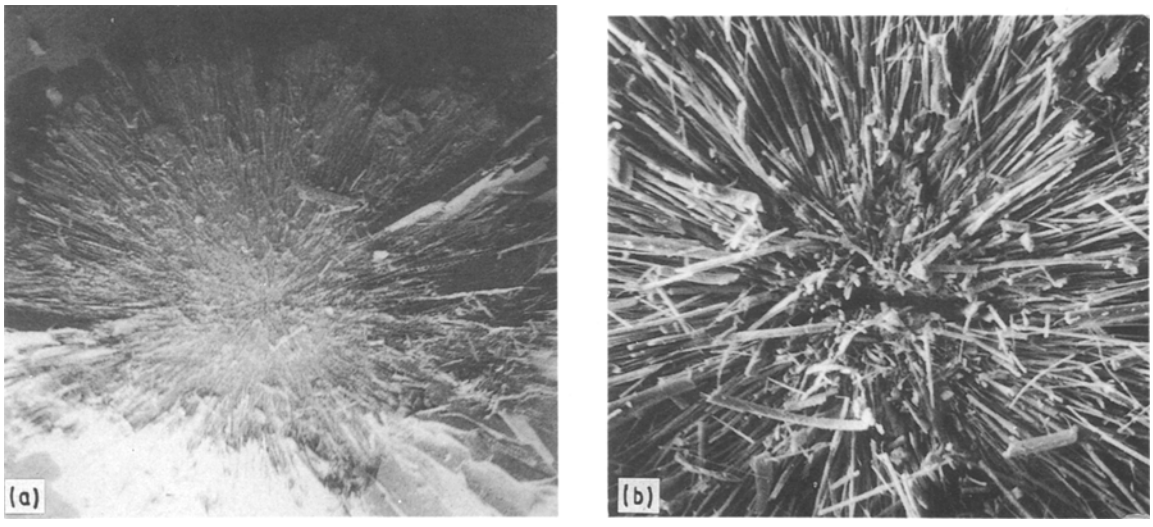

Figure 6 Scanning electron micrographs showing: (a) ST spherulite (× 20) and (b) central region of (a) (× 200).

hollow and there seems to be multiple nuclei around the central portion from where the crystal fibres diverge radially. This observation looks very similar to that of neodymium tartrate as reported by Kotru and Raina [24].

The coalesced spiky spherulites when observed under the SEM appear as shown in Fig. 7a. Here also the spherulites are composed of randomly oriented crystal needles as shown in a higher magnification scanning electron micrograph (Fig. 7b). The crystal needles have well-developed habit faces.

In order to know about the internal structure of the spherulites, their cross-sections were examined under SEM. The cross-sections were obtained by cutting the spherulite into two halves with the help of a sharp-edged knife. Fig. 8a shows two halves of an NT-spherulite thus obtained. A higher magnification electron micrograph revealing the texture of the surface of one of the halves is shown in Fig. 8b. The crystal fibres seem to diverge radially from the centre of the spherulite. A still higher magnification electron micrograph (Fig. 8c) of a region from Fig. 8b, illustrates the radial divergence of the fibres. Here it is undoubtedly clear that the whole NT-spherulite is not composed of randomly oriented crystallites as was the case with the spiky spherulites of Fig. 7a. It may be that initially, the development of NT-spherulites is because of crystal fibres diverging radially from the centre, but the subsequent development is due to

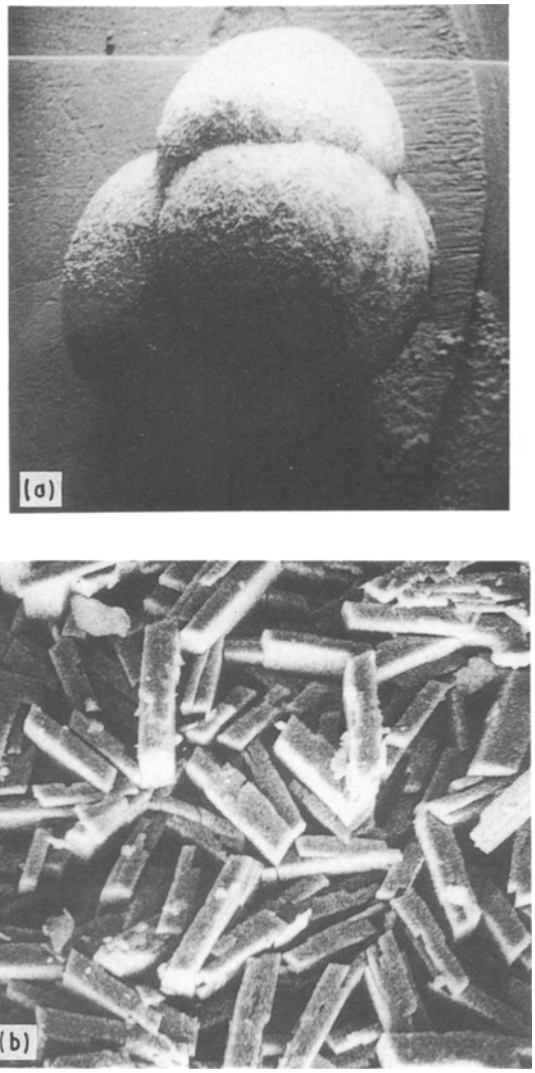

Figure 7 (a) SEM depicting coalesced spiky spherulite (× 20); (b) a portion of (a) at a higher magnification revealing the random pattern of needles (× 500).

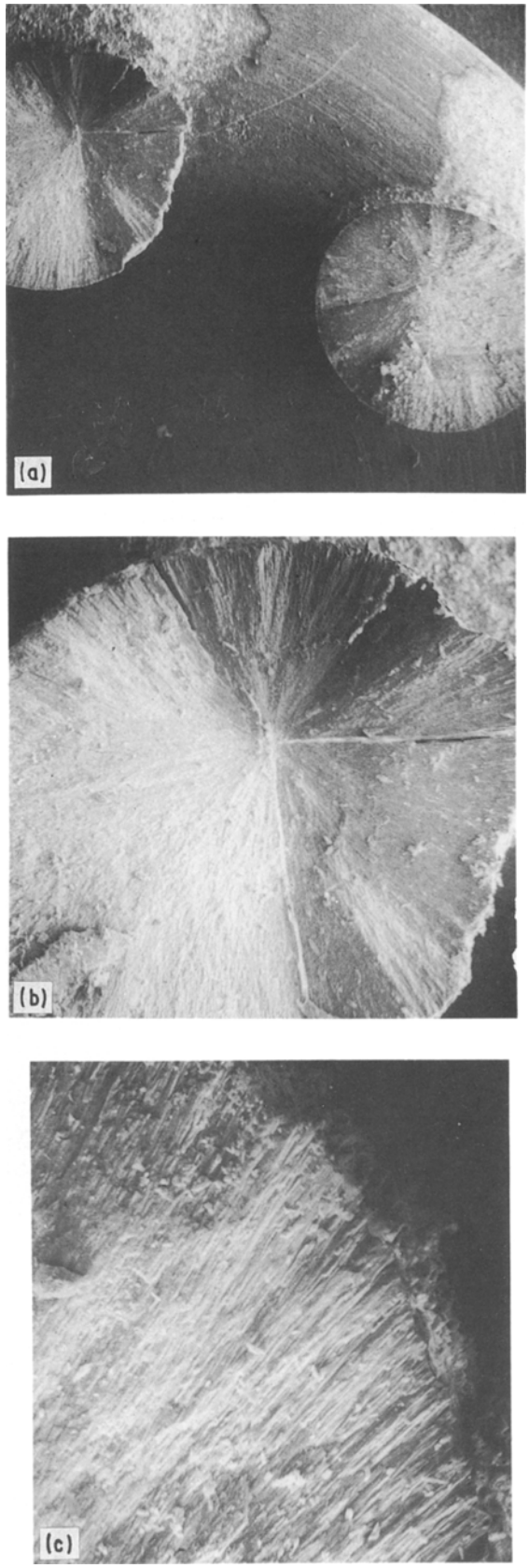

Figure 8 Scanning electron micrograph showing (a) sectioned halves of a normal spherulite (× 20); (b) the surface of one of the halves from (a) (× 50) and (c) a portion of (b) depicting the radial divergence of fibres (× 200).

crystallites growing in random orientations all over the spherulitic surface.

Fig. 9a illustrates one of the cleaved sections of a spiky spherulite. Only half of the cross-section was found as the remaining half was broken while handling. A close inspection reveals that the fibres do not originate from a common nucleus at the centre but instead diverge from several nuclei dispersed within a spherical region at the centre of the spherulite. The internal spherulitic constitution with regard to nucleus and crystal fibres appears to be very similar to the one observed by Kotru and Raina [24] for neodymium and didymium tartrate spherulites. The crystal fibres of the spiky spherulite of Fig. 9a are shown at a higher magnification in Fig. 9b. One such fibre which was separated from other fibres is shown at a higher magnification in Fig. 10. The fibres are actually elongated platelets and have a reasonably flat surface. Some needles (or what is termed as fibres) show a large number of smaller needles attached to their surfaces. Fig. 11 is one such surface of a longer needle where many smaller needles are attached to its surface.

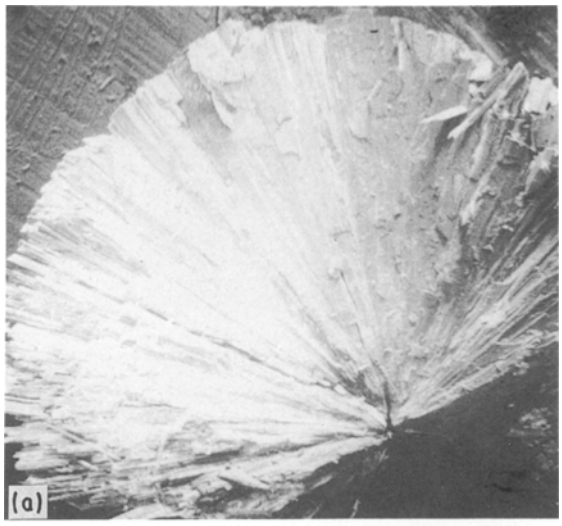

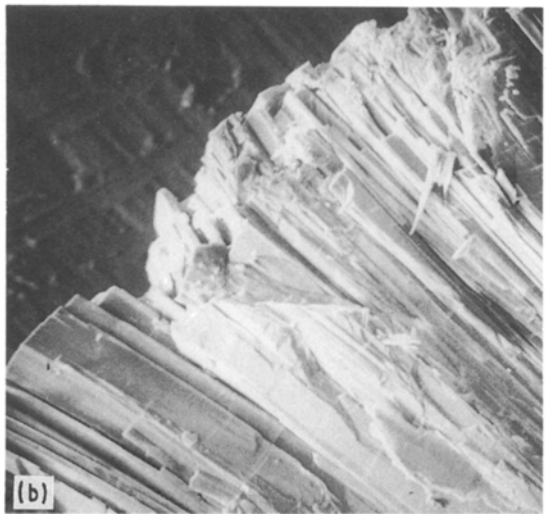

Figure 9 SEM illustrating (a) a cleaved section of a spiky spherulite (× 50) and (b) the fibres of a spiky spherulite from (a) at a higher magnification (× 200).

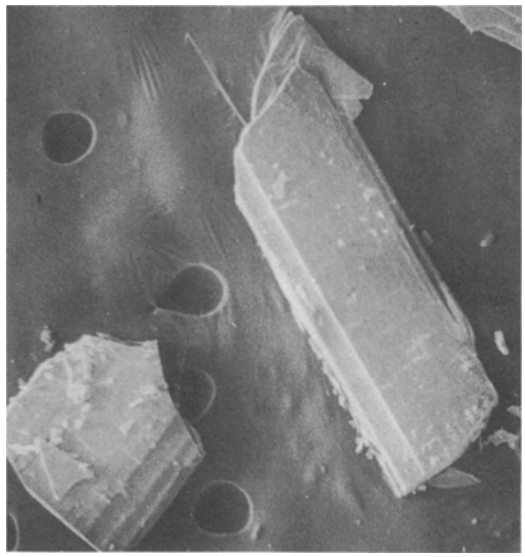

Figure 10 SEM showing needles at a higher magnification (× 100).

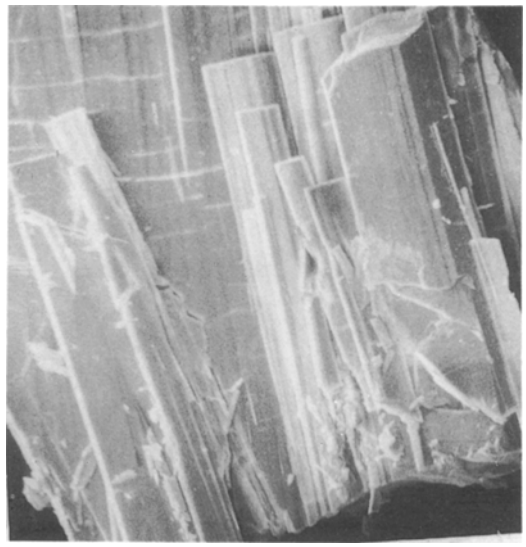

Figure 11 SEM showing a needle at a higher magnification. Many smaller needles can be seen attached to the surface (× 200).

3. Conclusions

1. The silica gel growth system involving the use of praseodymium nitrate as the top reactant and sodium metasilicate gel impregnated with tartaric acid as the lower reactant results in the spherulitic crystallization of praseodymium tartrate.

2. EDAX confirms the presence of Pr as the rare-earth constituent of the grown material. Infrared spectra establish the presence of carbon, oxygen and water of crystallization in the material. X-ray powder diffraction reveals the crystallinity of the material.

3. The chemical and thermogravimetric analyses suggest the gel grown praseodymium tartrate to be associated with 5 molecules of water of hydration. The formula of the grown material is thus $Pr_2(C_4H_4O_6)_3 \cdot 5H_2O$.

4. The results of thermal analysis suggest the gel-grown praseodymium tartrate to be thermally unstable even at low energies. The decomposition starts at

about 40 °C and the process continues up to 560 °C after which it reduces to Pr_2O_3. The comparison of the TG and DSC curves suggest the transformations (phases prior to Pr_2O_3) are associated with mass changes and there is no physical (crystallographic) transformation independent of mass change.

5. SEM studies confirm that the spiky spherulites are composed of fine crystal needles. The spherulitic growth is not as a result of radially diverging crystal fibres from a centrally located single (common) nucleus but instead is due to the development of crystal fibres from several nuclei dispersed within a spherical region at the centre of the spherulite.

Acknowledgements

The authors are grateful to Mr. V. G. Shah (Geo Fc) of PRL, Ahmedabad, for his assistance in SEM and EDAX facilities. We are also thankful to Mrs. V. V. Ghisas of NCL, Pune for the help rendered in recording the XRD patterns.

References

1. B. M. WANKLYN, *J. Cryst. Growth*, **5** (1969) 323.
2. B. M. WANKLYN and Z. HAUPTMAN, *J. Mater. Sci.* **9** (1974) 1073.
3. S. J. SURITHENBY, B. M. WANKLYN and M. R. WELLS, *ibid.* **9** (1974) 845.
4. B. M. WANKLYN, *J. Cryst. Growth* **37** (1977) 51.
5. S. H. SMITH and B. M. WANKLYN, *ibid.*, **21** (1974) 23.
6. B. M. WANKLYN, F. R. WONDRE, G. B. ANSELL and W. DAVISON, *J. Mater. Sci.* **9** (1974) 2007.
7. P. N. KOTRU and B. M. WANKLYN, *ibid.* **14** (1979) 755.
8. P. N. KOTRU, K. K. RAINA, S. K. KACHROO and B. M. WANKLYN, *ibid.* **19** (1984) 2582.
9. R. A. LEFEVER, J. W. TOEPY and A. B. CHASE, *J. Appl. Phys.* **32** (1961) 962.
10. S. S. GENDELEY and A. G. TITOVA, in "Growth of crystals" Vol. 9 (1975) edited by N. N. Sheftal and E. I. Givargizov, Bureau, New York and London, p. 90.
11. J. W. McCAULEY and H. M. GEHRHARDT, Tech. Report Number AMMRCTR 70-13 (Army Materials and Mechanics Research Centre, Watertown Mass) (June 1970) p. 1–21.
12. P. N. KOTRU, N. K. GUPTA and K. K. RAINA, *Cryst. Res. Technol.* **21** (1986) 15.
13. *Idem., J. Mater. Sci.* **21** (1986) 90.
14. *Idem., Cryst. Res. and Technol.* **22** (1987) 177.
15. P. N. KOTRU and K. K. RAINA, *J. Mater. Sci. Lett.* **5** (1986) 760.
16. P. N. KOTRU, N. K. GUPTA, K. K. RAINA and I. B. SHARMA, *J. Mater. Sci.* **21** (1986) 83.
17. P. N. KOTRU, K. K. RAINA and M. L. KOUL, *ibid.* **21** (1986) 3933.
18. *Idem., J. Mater. Sci. Lett.* **6** (1987) 711.
19. P. N. KOTRU and K. K. RAINA, *J. Appl. Phys.* **D19** (1986) L9.
20. P. N. KOTRU, N. K. GUPTA, K. K. RAINA and M. L. KOUL, *Bull. Mater. Sci.* **8** (1986) 547.
21. P. N. KOTRU, K. K. RAINA and M. L. KOUL, *Ind. J. Pure & Appl. Phys.* **25** (1987) 220.
22. V. MANSOTRA, K. K. RAINA and P. N. KOTRU, *J. Mater. Sci.* (communicated) 1990.
23. T. M. MAGUIRE, Private communication, 1988.
24. P. N. KOTRU and K. K. RAINA, *J. Cryst. Growth* **91** (1988) 221.

Received 25 June 1990
and accepted 31 January 1991